Network-Independent Grid Synchronous Stability Boundary and Spontaneous Synchronization

Yu Yuan *

Posted Date: 14 March 2024

doi: 10.20944/preprints202310.1791.v4

Keywords: Complex network; spontaneous synchronization; synchronous stability boundary

Article

Network-Independent Grid Synchronous Stability Boundary and Spontaneous Synchronization

Yu Yuan

Sichuan Technology & Business College; yuyuan.sctbc@outlook.com

Abstract: Spontaneous synchronization on complex networks is widespread in the real world. These synchronization behaviors are believed to be closely related to the network topology. However, it is difficult to obtain complete information in reality. Therefore, a network-independent analysis path is needed. In this study, a synchronized stability boundary equation is derived which is system- and disturbance-independent and applicable to arbitrarily coupled grids. The results also imply that spontaneous synchronization on a network may be network independent. These conclusions provide new research paths for network synchronization and analyze the synchronization stability of grids in a unified way.

Keywords: complex network; spontaneous synchronization; synchronous stability boundary

Introduction

The study of synchronization began with Huygens. With the rise of the study of collective behavior on complex systems, spontaneous synchronization in coupled systems has attracted public attention [1]. Synchronization in complex systems is widespread in the real world [1,2], e.g., the aggregation of flocks of birds and schools of fish, the flashing of fireflies, the synchronization of generators.

Currently, it is widely believed that network topology is closely related to spontaneous synchronization [2]. In order to analyze these spontaneous synchronization behaviors, the interactions between individuals are first simplified into a coupled complex network, and then studied using the knowledge of network synchronization. However, this is actually difficult to do [3]. Realistic interactions are often invisible, which may lead to incorrect network topologies. The complexity and nonlinearity of real networks can also make topological information incomplete [4]. Overly large networks make clear topology modeling very difficult. Therefore, the appropriate solution is to construct a network-independent synchronization analysis path that identifies the collective synchronization and which individuals are not in this collective only by the behavior of each individual in the system. In this study, this is experimentally verified on a realistic grid.

Synchronization is a prerequisite for the normal operation of a power grid [5]. Large power systems are complex coupled systems where uncertainties [6] and nonlinearities coexist. To analyze the stability of these systems, researchers have developed numerous insightful discriminatory methods [1,7–11], including finding stability region boundary [12–14] and describing the synchronization of generators using the spontaneous synchronization conditions of complex networks [2].

Finding the stability boundary of a system is an important fundamental problem [13,15,16]. The stable boundary is the union of unstable equilibrium points [17]. When an operating point is outside the boundary, the corresponding system is desynchronized [14]. The synchronous stability boundary, which is a core concept of grid stability, is closely related to many issues [18–20]. Therefore, studying synchronous stability boundary has a significant impact on the development of power systems. For decades, scientists and engineers have wanted to find an analytical equation to describe the boundary [12,13,21]. On the other hand, spontaneous synchronization on complex systems has been used to explain the synchronized operation of generators in interconnected grids [22]. Therefore, many studies on power system stability are based on the knowledge of synchronization conditions

 doi:10.20944/preprints202310.1791.v4

on complex networks [2,22]. However, this scheme is sometimes considered to oversimplify real systems [8,22], while arguing that self-organization does not exist in the grid case [8].

Here, an equation is derived and visualized to describe the stability boundary of the power system in a unified way. This equation proves that the synchronization stability boundary is independent of the network and disturbances. In addition, evidence that spontaneous synchronization occurs only at the boundary and manifests itself as a specific spatio-temporal structure was found in the study. This indicates that the synchronization conditions on the network are also independent of the network. In this context, for potential scenarios where it is difficult to construct network models, this research develops new method for synchronization on complex networks. This will analyze the synchronization of power grids in a unified way and will be instructive for other disciplines.

Stability Boundary

The New England test system (10-gen) was tested (Figure 1). A three-phase short circuit ground fault occurred at 18node. (see Supplementary Material for details)

Figure 1 shows that the synchronization stability boundary can distinguish between synchronized and desynchronized states and gives specific information about synchronized and desynchronized individuals or groups, respectively. This result suggests that the partial synchronization phenomenon [23–25] in which the two states coexist is caused by the loss of synchronization stability between these individuals or groups. The different synchronization patterns can be easily identified from figure. m operating points outside the boundary indicate that the n meta-generators are sequentially divided into m+1 synchronized groups. This can be directly applied to discriminate coherent generators [26].

Figures 1.(b), (c), and (e) show that the synchronization stability boundary can discriminate the stability of multiple swings for multiple generators in real time, which is a difficult and important problem [27]. For n-1 operating points of n generators, the system is considered to be out of global synchronization if any of the operating points (u_K, u_L, δ_{KL}) is outside the boundary and far from the other operating points ($\sigma_{\Delta t}(\delta_i) >> \sigma_{\Delta t-\varepsilon}(\delta_i), 0<\varepsilon<\Delta t$, where Δt is the fault duration) (Figure 1(b) and Figure 2(a)). The moment the operating point crosses the boundary (Figure 1(c)) is the moment of loss of synchronization (Figure 1(e)). The results of numerical experiments in Figure 1.(d) and (e) fit well with the results shown in Figure 1.(b) and (c).

Similar results are obtained on 3-generator test system (3-gen) by the same steps (see Supplementary Material for details). New England test system and 3-gen are two completely different network systems, but both apply the same boundary equation. These results show the validity of the boundary to discriminate the synchronization stability of the grid, and also demonstrate that the synchronization stability boundary is independent of the network topology.

u_i is the port bus voltage Per Unit of the ith generator, and $\delta_i = 2\arctan(\omega_i)$ is the angle of rotation rate of the ith generator. ω_i is the rotor speed Per Unit of the ith generator. $\delta_{KL} = |\delta_K - \delta_L| \geq 0$. Note that δ_i is not a phase. By the definition of synchronization, $\delta_1 = \delta_2 = \cdots = \delta_n$.

 doi:10.20944/preprints202310.1791.v4

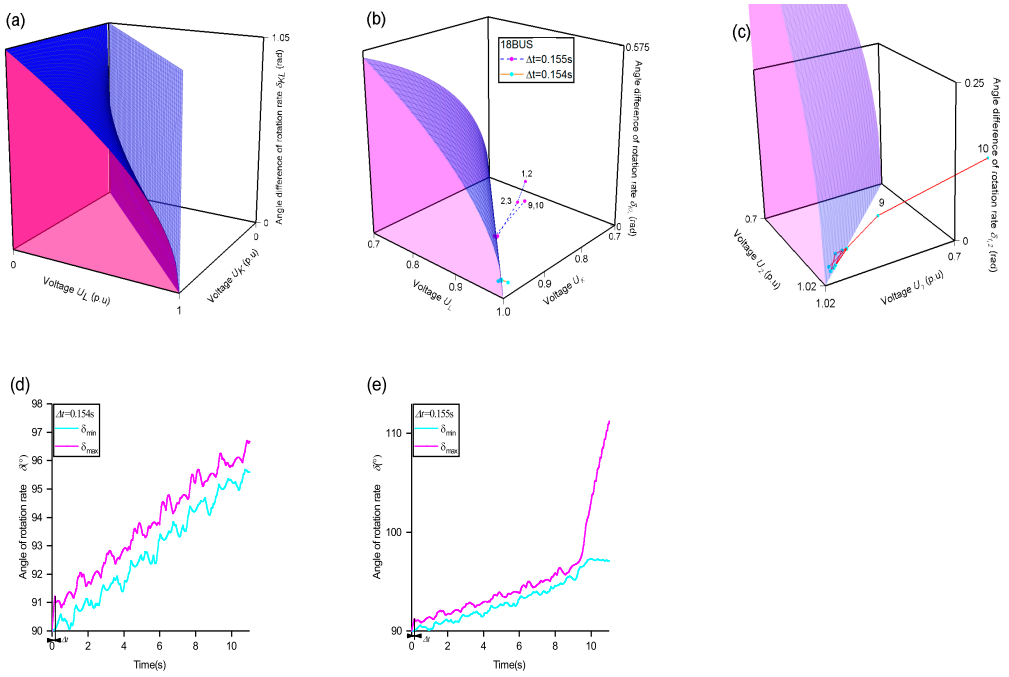

Figure 1. Stability boundary.

(a). Visualisation of the boundary. The stability boundary (blue surface) and $(0,u_l,\delta_{kl}),(u_k,0,\delta_{kl}),(u_k,u_l,0)$ (pink surface) together enclose the stability domain. The boundary equation is $|u_K|=|u_L|\cup\frac{|u_L|}{|u_K|}=2\cos\delta_{KL}-1$.

(b). Synchronization stabilization discrimination. At $\Delta t=0.154s$ and $\Delta t=0.155s$, respectively, this boundary strictly discriminates synchronization stability. The plane $|u_l|=|u_k|$ is not shown. At $\Delta t=0.154s$, all generators maintain synchronization stability. At $\Delta t=0.155s$, the system is partially synchronized. The meta-generators are sequentially divided into 4 groups.

(c). Multiswing stabilization discrimination ($\Delta t=0.155s$). Numbers 9 and 10 indicate period T_m after the fault, and $dT=1s$ (see Methods for details). The system is destabilised in the time interval $(9s,10s)$. The figure shows the trajectory of $(u_1,u_2,\delta_{1,2})$. The operating point crosses the boundary at the time of instability, and δ_{kl} rapidly increases after the voltage changes .

(d) and (e) are the results of numerical experiments. The maximum value of δ_i is represented by the pink curve and the minimum value by the blue curve. $\delta_{\min}\leqslant\delta_i\leqslant\delta_{\max}$. (d), δ_i of all generators are close to each other and have approximately the same rate of change. (e), in time interval $(9s,10s)$, $\delta_{\max}$ - $\delta_{\min}$ becomes sharply larger.

Regarding the synchronization, one different assumption than before [20]: the system requires the synchronous power $P_{u'}=\frac{|u'|^2}{|Z_{KL}|}$ to maintain synchronous stability, and the synchronous power is provided by the coupling power $P_{\Delta u}=\frac{|\Delta u|^2}{|Z_{KL}|}$ within the system, Z_{KL} is the impedance between the Kth and Lth meta-generators (see Supplementary Materials for details). Here, the coupling role is replaced by specific physical quantities and is variable. The amplitude (voltage in this case), which

 doi:10.20944/preprints202310.1791.v4

has been long neglected in the past for simplicity [28], actually plays a decisive role in synchronization stability.

$$|u_K| = |u_L| \cup \frac{|u_L|}{|u_K|} = 2\cos\delta_{KL} - 1, |u_K| > |u_L| \geq 0, \delta_{KL} \in \left[0, \frac{\pi}{3}\right] \quad (1)$$

Eq.(1) is the analytical equation for the synchronous stability boundary. Specifically, when $\delta_{KL} > 0$, the set where $|u_L| = |u_K|$ is the isolated stability domain [12]. This may explain why symmetric networks have better synchronization capabilities [22].

The current analysis for synchronous stability on a network requires the creation of a network coupling matrix and then the master stability equation [29]. This approach is mainly applicable to the case where the network topology is complete. In contrast to previous reports [2,12,13], Eq.(1) is independent of the network topology, system parameters, perturbations and the number of the subsystem. This shows that the stability boundary is independent of these factors. This provides the basis for the applicability of Eq.(1) to different grids(see Supplementary Material). Also this case demonstrates that synchronization of complex networks can be analyzed even without coupling matrix. These conclusions are proved by numerical experiments on different standard arithmetic models. (Figure 1(d), (e) and Supplemental Material Figure S4).

Eq.(1) has a variant as follows: $\delta_{KL}^{cr} = \arccos(1 - \frac{|u_K| - |u_L|}{2|u_K|})$.

When $|u_K|, |u_L|$ are sufficiently close [30], the stability margin of the Kth and Lth generator angle rate difference δ_{KL}^{cr} also tends to 0. This indicates that the system may already be in a critical state during normal operation. In this case, even if the difference in the values between δ_K and δ_L is small, it takes only a very small perturbation to make the system asynchronous [31,32]. As $|u_K| - |u_L|$ becomes larger, the stability margin δ_{KL}^{cr} increases. This explains the counterintuitive nature that the system has better synchronization stability when either highly symmetric($|u_L| = |u_K|$) or highly asymmetric [5,33].

As a result, Eq.(1) allows a unified analysis of the synchronization stability of the grid and provides a new understanding of synchronization.

Synchronization is a pervasive topic in other disciplines such as social networks, biological systems, brain neural networks and other physical systems [1]. In many cases, it is impractical to model a network with a clear topology. Here, the synchronization-stabilizing boundary equation for real networked systems, independent of network topology, is developed. This helps to open up new avenues for synchronization studies. For example, synchronization on networks can be studied with the help of the boundary by mapping changes in network topology to changes in operating points. Boundary equations in other fields may have different forms, which require further research.

Spontaneous Synchronisation

In order to study the process of desynchronization, the trajectories of the operating points near the critical point are investigated and found to exhibit a special spatio-temporal structure.

(a). $\sigma(\delta_i)$ is the standard deviation of δ. $\sigma(\delta_i)$ started to fall at 0.147s and rose by 1300% at 0.155s when the system became unstable.

(b). In the $\delta_1 - \delta_2$ plane, the operating points were in "decelerated motion" and appeared to be crossing the potential barrier before they reached the boundary. The elliptical area marks the position of the potential barrier. From 0.147s onwards the interval between operating points decreased in the direction of increasing Δt (shaded area).

 doi:10.20944/preprints202310.1791.v4

(c). In the $u_1 - u_2$ plane, the graph is a ring structure which appears at the same time as the potential barrier. The potential barrier and the cycle were the results of the self-organizing behavior in the $\delta_K - \delta_L$ and $u_K - u_L$ planes, respectively.

Modulus of the order parameter is $R = \left| \frac{1}{N} \sum_{j=1}^{n} \exp(i\delta_j) \right|$ [34]. R and $\sigma(\delta_i)$ are closely related. When $\sigma(\delta_i) = 0$, $R = 1$, the system is perfectly synchronized.

The decrease in $\sigma(\delta_i)$ from the highest point indicated that in the vicinity of the critical point, the system spontaneously directs the velocity of the subsystem to the mean value to increase R (Figure 2(a)). This can be interpreted as a spontaneous synchronization effect due to system coupling [7,34]. As the stability boundary is approached, the system self-organizes itself towards synchronous evolution [22]. Since $\sigma(\delta_i)$ is discontinuous on the boundary, it may also lead to R discontinuity (Figure 2(a)). Meanwhile spontaneous synchronization causes R to increase whether the running point crosses the potential barrier inward or outward. This indicates that the self-organizing behavior makes R inconsistent in different directions. This is similar to the hysteresis phenomenon of explosive synchronization [35,36].

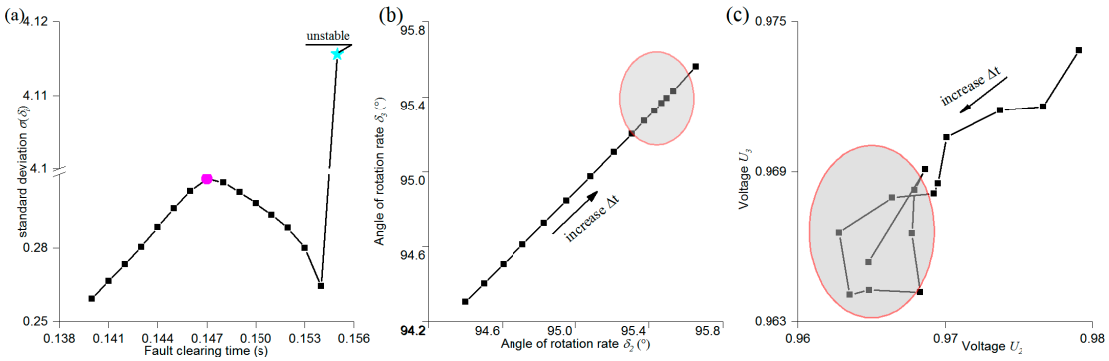

Figure 2. Boundary effects, with increased fault duration Δt from 0.140s to 0.154s ($d(\Delta t) = 0.001s$), and the trajectory of the disturbed operating point near the boundary. The arrow shows the direction of increase of Δt .(the 18node three-phase short circuit to ground fault).

Self-organizing behavior emerges from the interactions of these generators, leading to parameter changes, which are reflected in the perturbation trajectories at the operating point. When the conditions are correct, the trajectories emerge with a marvelous spatio-temporal structure. Although spontaneous synchronization has been used to understand the synchronous operation of generators [22], this structure has not been reported due to its elusive hiding near the critical point. Due to the presence of constraints, the perturbed trajectories of all the meta-generators take on this structure at the same time (Figure 3). This suggests that self-organizing behavior occurs simultaneously throughout the system.

 doi:10.20944/preprints202310.1791.v4

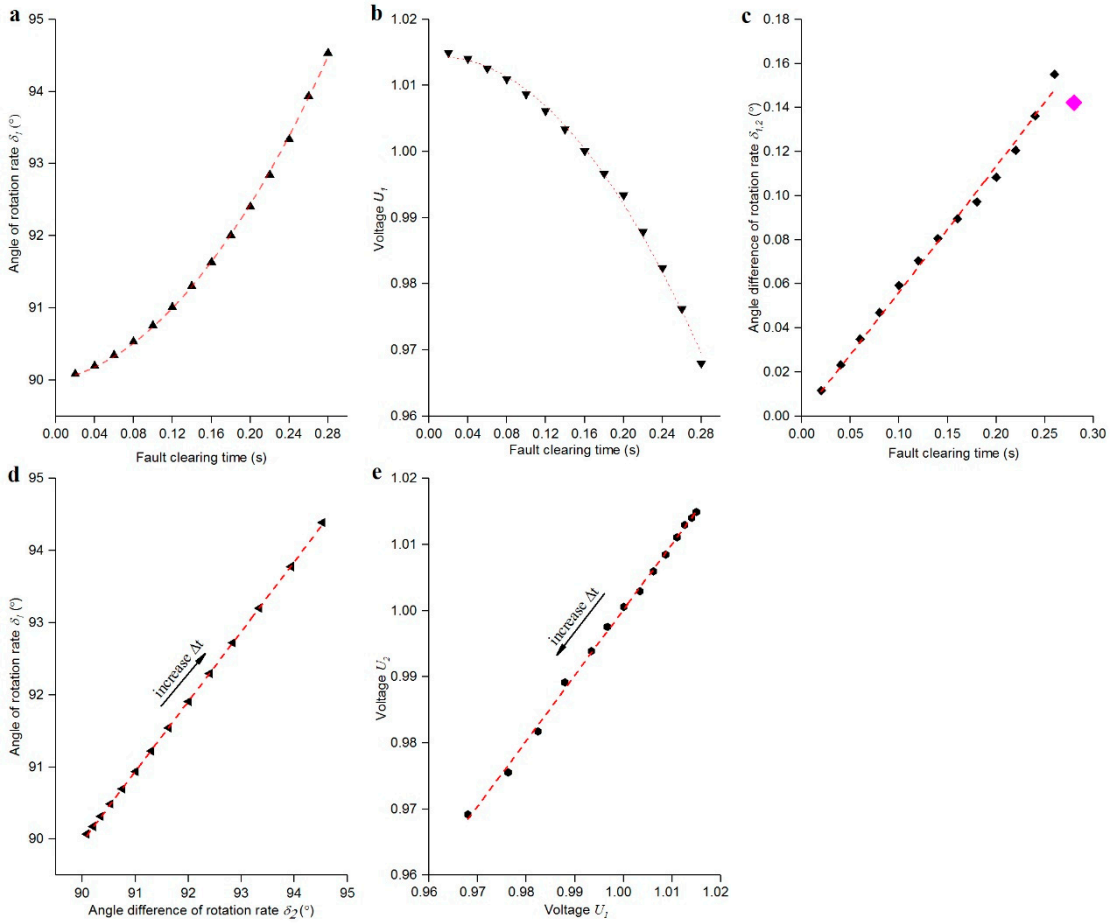

Figure 3. Fitting results for perturbed trajectories of a 12-node trajectory of disturbed operating points after a three-phase short circuit to ground fault. ($d(\Delta t) = 0.02s$).

Spontaneous synchronization is considered to be the onset of network synchronization [1]. Currently, spontaneous synchronization is considered to be closely related to network topology [37]. Here, experimental results show that spontaneous synchronization occurs on the synchronization stability boundary. (Figure 2 and Figure S7). For coupled network systems, this strong correlation indicates that the location where spontaneous synchronization occurs is also determined in $u_K - u_L - \delta_{KL}$ by Eq.(1) [2,22]. This may indicate that the mechanism of spontaneous synchronization is not necessarily related to the network topology, i.e., synchronization on the network may be independent of the network [29,38,39]. This will challenge the traditional perception of synchronization in networks. At the same time, it also implies that there may be a potentially close relationship between the critical stability of the dynamical system and the Self-organized behavior.

The behavior of the operating point near the boundary is very complex. For example, it does not always result in the formation of a potential barrier (see Figure S6). The reasons for this difference, or rather, the specific conditions for the formation of this particular structure of potential barrier and more information awaits further research.

Dynamic Processes at Disturbed Operating Points in the Coordinate System $u_K - u_L - \delta_{KL}$

Of greater concern to power system decision makers is how much stability margin is left in the disturbed system.

 doi:10.20944/preprints202310.1791.v4

To understand the behavior of the power system after a disturbance and to calculate the critical clearing time (CCT) and the controlling unstable equilibrium point (UEP), it is necessary to study the perturbation trajectories consisting of running points.

In the expressions, (i) denotes the ith meta-generator, and $i=1,\cdots,k,l,\cdots,n$. The subscripts u and ω denote the coefficients of the meta-generators at $u_i-\Delta t$ and $\delta_i-\Delta t$, respectively. $\Delta T'$ is the starting fault duration at which self-organised behaviour occurs at the disturbed operating point. To make it easier to show the details, δ_{kl} in the picture uses the angle system. δ_0 and u_0 are the initial values when $\Delta t=0$. a and V denote the acceleration and velocity of the operating point about Δt, respectively.

a. The projection of the disturbed trajectory in the $\delta_1-\Delta t$ plane, fitted using the equation . $\delta_i=\frac{a_\omega(i)}{2}*\Delta t^2+V_\omega(i)*\Delta t+\delta_0(i),\Delta t\in(0,\Delta T']$

b. The projection of the disturbed trajectory in the $u_1-\Delta t$ plane, fitted using the equation . $u_i=\frac{a_u(i)}{2}*\Delta t^2+V_u(i)*\Delta t+u_0(i),\Delta t\in(0,\Delta T']$

c. The projection of the disturbed trajectory in the $\delta_{1,2}-\Delta t$ plane, fitted using the equation $\delta_{kl}=\delta_k-\delta_l=\frac{a_{kl}}{2}*\Delta t^2+V_{kl}*\Delta t,\Delta t\in(0,\Delta T']$. Notably, $\delta_{1,2}$ descended at $\Delta t=0.28s$.

d. The projection of the disturbed trajectory in the $\delta_1-\delta_2$ plane, fitted using the equation $\delta_k=a_\delta*\delta_l+b_\delta,\Delta t\in(0,\Delta T']$, where $\delta_k>\delta_l,a_\delta>1$.

e. The projection of the disturbed trajectory in the u_1-u_2 plane, fitted using the equation $u_k=a_u*u_l+b_u,\Delta t\in(0,\Delta T']$.

Figure 3.a and 3.b show that the operating points move with a uniformly variable speed before the system becomes unstable.

Contrary to intuition [40], δ_{12} suddenly dropped at $\Delta t=0.28s$ (Figure 3.c). This anomaly suggested that the system appears to have a tendency to maintain its own stability.

Figure 3.d and E show that the perturbed trajectories of the subsystems of the coupled system are linearly correlated in the stability domain. This indicates that for a determined power grid, each perturbed trajectory has almost the same T_i' (For the 3-gen system, $\frac{\left|\Delta T_\alpha'-\Delta T_\beta'\right|}{\min(\Delta T_\alpha',\Delta T_\beta')}\le 2.6\%$ in Table S1). The effects of perturbations are global, reflecting the challenges of controlling the stability of complex systems [41–43].

When a high degree of accuracy of the results is not needed, $a_{KL}=0$. The following expression can be derived: $\Delta T'=\frac{2\left|V_{KL}-(a_\delta-1)V_\omega(i)\right|}{(a_\delta-1)a_\omega(i)},i=2,3,\cdots,n$

This can be used to easily and quickly check the stability margin of the system after a disturbance [44]. By approximating $\Delta T'$ as the CCT [21,44], the coordinates of the critical stable operating point $(u_K^{cr},u_L^{cr},\delta_{KL}^{cr})$ and critical rate of the meta-generator l in the current system can also be estimated [45].

 doi:10.20944/preprints202310.1791.v4

$$u_i^{cr} = \frac{a_u(i)}{2}\Delta T'^2 + V_u(i)\Delta T' + u_0(i)$$

$$\delta_{KL}^{cr} = V_{KL}\Delta T' = \arccos\left(1 - \frac{|u_K| - |u_L|}{2|u_K|}\right)$$

$$\delta_L^{cr} = \frac{a_\omega(L)}{2}\Delta T'^2 + V_\omega(L)\Delta T' + \delta_0(L) = \frac{\arccos\left(\frac{|u_K| - |u_L|}{2|u_K|}\right) - b_\delta}{a_\delta - 1}$$

$$\omega_L^{cr} = \tan\frac{\delta_L^{cr}}{2}$$

In summary, the CCT and UEP can be calculated using only information about the rotation rate [11], but considering only a single information source may result in more errors. Theoretically, using $\Delta T'$ directly as the CCT would also lead to a conservative result. (Extended Data Table 1 can be referenced for more details).

The equation of motion for R is: $R(\Delta t) = \left|\frac{1}{N}\sum_{j=1}^{n}\exp\left[i\delta_j(\Delta t)\right]\right|$.

The current power system is receiving an increasing number of renewable energy sources. These sources are connected to the power grid via inverters, which may change the inertia of the system [46–48], complicating the coefficients. This issue should be further studied.

On a finer scale, the operating points near the stability boundary exhibit unusual behavior (Figure 2).

When $\frac{d^2\delta_L}{d(\Delta t)^2} = a_\omega(i) < 0$ and a_δ is constant, the trajectories exhibit a marvelous spatio-temporal structure (Figure 2(b) and (c)). Due to the constraint $\delta_K = a_\delta * \delta_L + b_\delta, \Delta t \in (0, \Delta T']$ and the same $\Delta T'$, the perturbed trajectories of all meta-generators simultaneously exhibit this structure.

Conclusions

In this study, a graceful stabilizing boundary equation that accurately describes an ideal synchronous stabilizing boundary is derived. Since the physical quantities in the equation are independent of the network, it is universally applicable to almost any power network. Therefore, the synchronization stability of the grid can be analyzed in a uniform way. It is also shown in a seminal way that the mechanism of synchronization may not be linked to the network topology and parameters. The experimental data are derived from simulations of the IEEE standard arithmetic models. The self-organizing behavior at the operating point demonstrates the existence of spontaneous synchronization on the boundary of the synchronization stability domain, which helps to confirm the argument that spontaneous synchronization is directly equivalent to synchronization stability. Additionally, the self-organizing behavior suggests the existence of a new explanation for the origin of the grid synchronous stability boundary. The concise mathematical tools, simple and universal methods, and ability to assess synchronization stability by simply monitoring the voltage and angular velocity provide great convenience for engineering applications. It is also demonstrated that synchronous stability studies of other coupled systems without clear network details can be performed by finding the correct parameters to directly derive the stability boundary while eliminating the need to construct elaborate network models. Finally, the behavior of the real system's operating points near the boundary is still very complex. It is still difficult to accurately predict these results, such as the specific conditions and duration of the occurrence of potential barrier structures, which require further exploration.

 doi:10.20944/preprints202310.1791.v4

Methods

Power-Grid Datasets

Here, I describe the sources of data for the two power-grid networks considered (3-generator test system (3-gen) and New England test system (10-gen) [5,49,50].

Definition and Diagram of Symbols

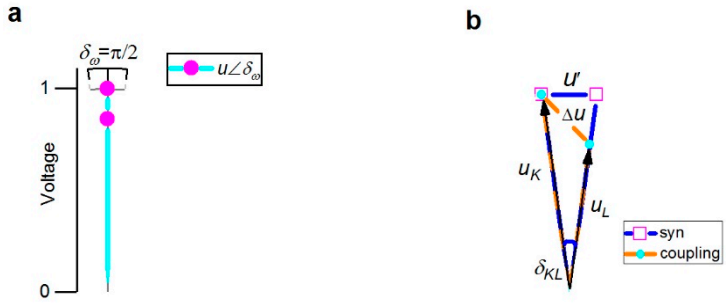

Figure 1. Schematic diagram of the power system operating coordinate system (U,δ_ω).

a. Synchronised system operation before disturbance, $\omega_1=\omega_2=\cdots=\omega_n=1$ and $\delta_i=2\arctan(\omega_i)=\frac{\pi}{2},i=1,2,\cdots,n$. The magenta dot indicates the operating point of the generator: (U,δ_ω).

b. The angle of rotation rate of the subsystems differ after the disturbance. u_K,u_L are the per unit voltage of the port bus of the Kth and Lth generators, respectively, $\delta_{KL}=|\delta_K-\delta_L|\geq 0$ is the difference in the angle of rotation rate between the Kth and Lth generators. Δu is defined as the coupling potential difference between generators Kth and Lth (yellow dotted line between Cyan dots). Correspondingly, u' is constructed to describe the synchronous potential difference between generators Kth and Lth (solid blue line between magenta square dots).

Extensive interconnections between generators would make stability analysis very difficult(see Figure S1). To solve this problem, the concept of a meta-generator is introduced here. At moment t, the instantaneous values of the n generators system $(u_i'(t),\delta_i'(t)),i\in(1,2,...,n)$ are arranged in descending order by δ_ω, relabelled, and then reconstituted as the n meta-generator system $(u_i(t),\delta_i(t)),i\in(1,2,...,n)$.

Data Sources and Experimental Procedures

In this study, the New England test system and 3-generator test system (Figures S4,S5,S6) were used. The two models are simulated separately using a simulation software package. Here, the fault was set as a three-phase short circuit to ground. The disturbed operating point of each generator was calculated. To observe the movement pattern of the disturbed operating points, the parameters of the control elements are set to 0.

In advance, the fault location was fixed, and the fault duration Δt was set. This experiment simulated the rotation rate $\omega_i'(t)$ and port bus voltage $u_i'(t)$ of the ith generator after different disturbances. Then, the angle of rotation rate of the ith generator $\delta_i(t)$ was calculated. Δt was increased in a fixed step length and $u_i'(t)$, $\delta_i(t)$ were calculated again until the system was destabilised. The faulty position was replaced, and the above steps were repeated.

 doi:10.20944/preprints202310.1791.v4

Subsequently, $(u_i'(t),\delta_i'(t)), i\in(1,2,...,n)$ was arranged and relabelled as $(u_i(t),\delta_i(t)), i\in(1,2,...,n)$. This was then averaged as follows:

The mean of $(u_i(t),\delta_i(t)), i\in(1,2,...,n)$ over $[0,T]$ was found: $u_i=\frac{1}{T}\int_0^T u_i(\tau)d\tau$ and $\delta_{KL}=\frac{1}{T}\int_0^T \delta_{KL}(\tau)d\tau=\frac{1}{T}\int_0^T \left|\delta_K(\tau)-\delta_L(\tau)\right|d\tau=\frac{1}{T}\int_0^T \delta_K(\tau)-\delta_L(\tau)d\tau=\delta_K-\delta_L$.

The mean of $(u_i(t),\delta_i(t)), i\in(1,2,...,n)$ over $[T_m,T_m+dT]$ was also found: $\delta_i(t_m)=\frac{1}{dT}\int_{T_m}^{T_m+dT}\delta_i(\tau)d\tau, U_i(t_m)=\frac{1}{dT}\int_{T_m}^{T_m+dT}U_i(\tau)d\tau, \delta_{kl}(t_m)=\delta_k(t_m)-\delta_l(t_m)$ There are several definitions of mean, and the simplest, i.e., the arithmetic mean, was used here.

This work added adjacent meta-generator data (u_K,u_L,δ_{KL}) and $(u_K(t_m),u_L(t_m),\delta_{KL}(t_m))$ to the coordinate system $u_K-u_L-\delta_{KL}$ to assess the system stability (Figure 1(b)) and time intervals of instability (T_m,T_m+dT) (Figure 1(d)).

An expression was fitted with Δt as the independent variable and $u_K,u_L,\delta_K,\delta_L,\delta_{KL}$ as the dependent variable (Figure 3). The critical clearing time (CCT) and the unstable equilibrium point (UEP) were then calculated.

Near the boundary, $\sigma(\delta_i),\delta_i,u_i$ was calculated at a finer scale.

Derivation of the Boundary Equation

As shown in Figure 1, $\Delta u=\sqrt{u_k^2+u_l^2-2u_ku_l\cos\delta_{kl}}$, $u'=\sqrt{2u_k^2(1-\cos\delta_{kl})}$.

Following the form of power in electricity $P=\frac{U^2}{R}$, the coupling power $P_{\Delta u}=\frac{|\Delta u|^2}{|Z_{KL}|}$ is defined to characterise the coupling between the meta-generators. To describe the energy required for the generator to maintain synchronous stability, the synchronous power is constructed: $P_{u'}=\frac{|u'|^2}{|Z_{KL}|}$. Z_{KL} is the impedance between the Kth and Lth meta-generators.

When the system is synchronized, the meta-generators are not in balance and are still coupled ($\delta_{KL}=0,u'=0,\Delta u=u_K-u_L\neq 0$). When the system is disturbed, δ_{KL} increases from 0, u' increases from 0, and Δu changes. When the coupling power between the two meta-generators is sufficient to provide synchronous power, i.e., $|P_{u'}|\le|P_{\Delta u}|$, the system is synchronous and stable. Conversely, when $|P_{u'}|>|P_{\Delta u}|$, there is not enough coupling power to maintain synchronization, and the system is unstable. It is observed that $\frac{|P_{u'}|}{|P_{\Delta u}|}=1\Leftrightarrow\frac{|u'|}{|\Delta u|}=1$. The set of points where $|u'|=|\Delta u|$ is the synchronous stability boundary.

In summary, $f(u_K,u_L,\delta_{KL})=\frac{|u'|}{|\Delta u|}=1$ is the system stability boundary equation. When $\frac{|u'|}{|\Delta u|}<1$, the system is stable. When $\frac{|u'|}{|\Delta u|}>1$, the system is unstable. Geometrically, $f(u_K,u_L,\delta_{KL})=1$ describes a curved surface that, together with $(0,u_L,\delta_{KL}),(u_K,0,\delta_{KL}),(u_K,u_L,0)$, encloses a stable domain. In summary, the boundary equation

 doi:10.20944/preprints202310.1791.v4

$|u_K| = |u_L| \cup \frac{|u_L|}{|u_K|} = 2\cos\delta_{KL} - 1$ can be found, where $|u_K| \geq |u_L| \geq 0, \delta_{KL} \in [0, \frac{\pi}{3}]$. The coordinate system $u_K - u_L - \delta_{KL}$ is established, and the boundary is visualized(Figure 1).

To determine the stability of a power system of n generators, only n pairs of variables $u_i, \delta_i, i \in (1,2,...,n)$ are needed, which are physically meaningful and easily obtainable.

Fitting of Operating Points to Trajectories

The intersection of the disturbed trajectory with the stability boundary is the unstable equilibrium point (UEP), and the failure time of the operating point along the disturbed trajectory to reach the UEP is the CCT. To calculate these important results, it is necessary to fit the disturbed trajectory to the kinematic expression in the (u, δ_ω) coordinate system. The variables of the operating point obtained from the simulation are fed into commercial software to fit the expression of the disturbed operating point.

Operating Point Behaviour on the Boundary

$\frac{d\delta_{KL}}{d(\Delta t)}$ is the derivative of δ_{KL} of the meta-generators with respect to Δt. Near the boundary, the derivative of $\frac{d\delta_{KL}}{d(\Delta t)}$ of the partial meta-generators changes from positive to negative (Figure 3). For this unusual phenomenon, on a finer scale, $(u_i(t), \delta_i(t)), i \in (1,2,...,n)$ is calculated sequentially for different Δt. The standard deviation of δ_i is calculated separately (Figure.2):

$$\sigma(\delta_i) = \sqrt{\frac{\sum_{i=1}^{n}(\delta_i - \mu(\delta_i))^2}{n}}, \mu(\delta_i) = \frac{\sum_{i=1}^{n}\delta_i}{n}.$$

a and b correspond to New England test system, generator disturbed instability process Schematic diagram of the disturbed trajectory of the operating point crossing the boundary after a three-phase short-circuit ground fault at 12-node and 18-node in node IEEE39 with gradually increasing Δt, respectively. (Δt increases from 0.04s, until destabilization)

The expressions for the disturbed operating points of the meta-generators and generators have the same form before and after permutation.

a. The projection of the disturbed trajectory in the $\delta_{39} - \Delta t$ plane. The result of the fit is $\frac{a_\omega(1)}{2} = 48.96109 \pm 0.79143, b_\omega(1) = 0.52556 \pm 0.17753, c_\omega(1) = 90$, and the adjusted R-squared value is 1.

b. The projection of the disturbed trajectory in the $u_{39} - \Delta t$ plane. The result of the fit is $\frac{a_u(1)}{2} = -0.2968 \pm 0.00968, b_u(1) = 0.01069 \pm 0.00299$ and the adjusted R-squared value is 0.99905.

c. The projection of the disturbed trajectory in the $\delta_{39,30} - \Delta t$ plane. The result of the fit is $a_{12} = -0.01545 \pm 0.00238, b_{12} = 0.02222 \pm 5.34533E\text{-}4$ and the adjusted R-squared value is 0.9993.

 doi:10.20944/preprints202310.1791.v4

d. The projection of the disturbed trajectory in the $\delta_{30}-\delta_{39}$ plane. The result of the fit is $a_\delta = 1.00019 \pm 3.59019\text{E-}4, b_\delta = \text{-}0.01749 \pm 0.03285$ and the adjusted R-squared value is 1.

e. The projection of the disturbed trajectory in the $u_{30}-u_{39}$ plane. The result of the fit is $a_v = 1.59015 \pm 0.00611, b_v = \text{-}0.59037 \pm 0.00625$ and the adjusted R-squared value is 0.99981.

The 18-node three-phase short-circuit ground fault, increase in fault time Δt from 0.140s to 0.154s, and the trajectory of disturbed operating point near the boundary. The arrow shows the direction of increase of Δt. The generator has the same barrier and attractor as the meta-generator.

a. In the $\delta_{32}-\delta_{34}$ plane, running points appear to cross the barrier before they reach the boundary, and the elliptical area marks the position of the barrier. From 0.147s onwards the interval between running points decreases in the direction of increasing Δt

b. In the $u_{32}-u_{34}$ plane, the graph is presented as a critical state local attractor, which appears simultaneously with the synchronous barrier. The ellipse indicates the position of the attractor. The graph of the trajectory of the run point from 0.147s onwards is shown as an attractor (in the shaded area).

The perturbed trajectory of the generator shows the same result at the same time.

a. The same boundary equation applise to the 3-gen system. 4-node sets the location of the operating point after a three-phase short-circuit ground fault.

b. Results of the multiswing instability for Δt=0.245s.

c and d are the results of the 4-node three-phase ground fault simulation, respectively. It is synchronization at $\Delta t = 0.244s$, out-of-Sync at $\Delta t = 0.245s$, and out-of-Sync in $(4s,5s)$.

Fitting results for perturbed trajectories for the 4-node trajectory of disturbed operating points after a three-phase short-circuit ground fault..

a. The projection of the disturbed trajectory in the $\delta_1 - \Delta t$ plane. The result of the fit is $\frac{a_\omega(1)}{2} = 263.16677 \pm 27.27487, b_\omega(1) = \text{-}12.16449 \pm 5.45497, c_\omega(1) = 90$. The adjusted R-squared value is 0.99997.

b. The projection of the disturbed trajectory in the $u_1 - \Delta t$ plane. The result of the fit is $\frac{a_u(1)}{2} = \text{-}4.32887 \pm 0.74225, b_u(1) = 0.63292 \pm 0.21231, c_u(1) = 1.00743 \pm 0.01298$, and the adjusted R-squared value is 0.97679.

c. The projection of the disturbed trajectory in the $\delta_{12} - \Delta t$ plane. The result of the fit is $a_{12} = \text{-}0.01956 \pm 0.03364, b_{12} = 0.06242 \pm 0.00673$, and the adjusted R-squared value is 0.99519.

d. The projection of the disturbed trajectory in the $\delta_1 - \delta_2$ plane. The result of the fit is $a_\delta = 1.05168 \pm 0.01287, b_\delta = \text{-}4.40363 \pm 1.21501$, and the adjusted R-squared value is 0.99925.

e. The projection of the disturbed trajectory in the $u_1 - u_2$ plane. The result of the fit is $a_v = 0.98731 \pm 0.00722, b_v = 0.01791 \pm 0.00713$, and the adjusted R-squared value is 0.99973.

a. The standard deviation of δ decreases from Δt=0.227s. It rises by 2200% at Δt=0.245s, where there is an instability.

 doi:10.20944/preprints202310.1791.v4

b. Derive $\frac{d\delta_{kl}}{d(\Delta t)}=\frac{d((a_\delta-1)\delta_l+b_\delta)}{d(\Delta t)}=(a_\delta-1)*\frac{d\delta_l}{d(\Delta t)}$ from the fitted equation (e). Due to the monotonicity of δ_i with respect to Δt, i.e. $\frac{d\delta_l}{d(\Delta t)}>0, \Delta t\in(0,CCT)$, $a_\delta-1$ changes from positive to negative and a_δ changes from greater than 1 to less than 1.

A three-phase short-circuit ground fault is set at the corresponding node. a, b, c, d, e correspond to the critical behaviour of the operating points after the failure of 6-node, 12-node, 24-node, 30-node & 36-node respectively. All the results show that near the boundary, there is always a significant decrease in $\sigma(\delta_i)$. These results demonstrate a strong correlation between synchronisation stability boundary and spontaneous synchronisation.

f and g show that the behaviour of the operating points also show the phenomenon of synchronous barrier when faults are set at 6-node and 24-node (shaded area).

The meta-generator operating point data $(u_1,u_2,\delta_{1,2})$ and $(u_2,u_3,\delta_{2,3})$ are substituted into equation 3) to obtain $\Delta T'_\alpha$, $\Delta T'_\beta$ respectively. Substitute $\Delta T'_\alpha$ and $\Delta T'_\beta$ into equation 4) to obtain $\delta_2^{cr}(\Delta T'_\alpha)$ and, $\delta_3^{cr}(\Delta T'_\beta)$ respectively. CCT(sim) is obtained from professional software simulation. $\delta_2(sim)$ and $\delta_3(sim)$ are the simulation values of δ_2 and δ_3, respectively. Notably, only a single piece of information from δ_l is used to calculate δ_i^{cr} here, so it adds to the error.

Supplementary Materials: The following supporting information can be downloaded at the website of this paper posted on Preprints.org.

Data Availability: All the data that support the findings of this study are available at Figshare (DOI:10.6084/m9.figshare.23585961).

Conflicts of Interest: The author declare no conflicts of interest.

References

1. A. A. Koronovskii, O. I. Moskalenko, and A. E. Hramov, *Synchronization in Complex Networks*, Tech. Phys. Lett. **38**, 924 (2012).
2. F. Dörfler, M. Chertkov, and F. Bullo, *Synchronization in Complex Oscillator Networks and Smart Grids*, Proc. Natl. Acad. Sci. U. S. A. **110**, 2005 (2013).
3. L. L. Linyuan and T. Zhou, *Link Prediction in Complex Networks: A Survey*, Phys. A Stat. Mech. Its Appl. **390**, 1150 (2011).
4. Y. Xu, W. Zhou, and J. Fang, *Topology Identification of the Modified Complex Dynamical Network with Non-Delayed and Delayed Coupling*, Nonlinear Dyn. **68**, 195 (2012).
5. F. Molnar, T. Nishikawa, and A. E. Motter, *Asymmetry Underlies Stability in Power Grids*, Nat. Commun. **12**, 1 (2021).
6. I. Martínez, A. R. Messina, and V. Vittal, *Normal Form Analysis of Complex System Models: A Structure-Preserving Approach*, IEEE Trans. Power Syst. **22**, 1908 (2007).
7. L. Zhu and D. J. Hill, *Synchronization of Kuramoto Oscillators: A Regional Stability Framework*, IEEE Trans. Automat. Contr. **65**, 5070 (2020).
8. M. R. Casals, S. Bologna, E. F. Bompard, G. D', N. A. Agostino, W. Ellens, G. A. Pagani, A. Scala, and T. Verma, *Knowing Power Grids and Understanding Complexity Science*, Int. J. Crit. Infrastructures **11**, 4 (2015).
9. G. Gurrala, A. Dimitrovski, S. Pannala, S. Simunovic, and M. Starke, *Parareal in Time for Fast Power System Dynamic Simulations*, IEEE Trans. Power Syst. **31**, 1820 (2016).
10. G. Gurrala, D. L. Dinesha, A. Dimitrovski, P. Sreekanth, S. Simunovic, and M. Starke, *Large Multi-Machine Power System Simulations Using Multi-Stage Adomian Decomposition*, IEEE Trans. Power Syst. **32**, 3594 (2017).
11. B. Wang, B. Fang, Y. Wang, H. Liu, and Y. Liu, *Power System Transient Stability Assessment Based on Big Data and the Core Vector Machine*, IEEE Trans. Smart Grid **7**, 2561 (2016).
12. Y. Yu, Y. Liu, C. Qin, and T. Yang, *Theory and Method of Power System Integrated Security Region Irrelevant to Operation States: An Introduction*, Engineering **6**, 754 (2020).

13. P. Yang, F. Liu, W. Wei, and Z. Wang, *Approaching the Transient Stability Boundary of a Power System: Theory and Applications*, IEEE Trans. Autom. Sci. Eng. 1 (2022).
14. E. A. Al-Ammar and M. A. El-Kady, *Application of Operating Security Regions in Power Systems*, IEEE PES Transm. Distrib. Conf. Expo. Smart Solut. a Chang. World (2010).
15. P. Kundur et al., *Definition and Classification of Power System Stability*, IEEE Trans. Power Syst. **19**, 1387 (2004).
16. B. B. Student Member and G. A. Senior Member, *On the Nature of Unstable Equilibrium Points in Power Systems*, IEEE Trans. Power Syst. **8**, 738 (1993).
17. H. D. Chiang, F. F. Wu, and P. P. Varaiya, *A BCU Method for Direct Analysis of Power System Transient Stability*, IEEE Trans. Power Syst. **9**, 1194 (1994).
18. K. N. Shubhanga and A. M. Kulkarni, *Application of Structure Preserving Energy Margin Sensitivity to Determime the Effectiveness of Shunt and Serles FACTS Devices*, IEEE Power Eng. Rev. **22**, 57 (2002).
19. P. Bhui and N. Senroy, *Real-Time Prediction and Control of Transient Stability Using Transient Energy Function*, IEEE Trans. Power Syst. **32**, 923 (2017).
20. H. H. Al Marhoon, I. Leevongwat, and P. Rastgoufard, *A Fast Search Algorithm for Critical Clearing Time for Power Systems Transient Stability Analysis*, 2014 Clemson Univ. Power Syst. Conf. PSC 2014 (2014).
21. D. Rimorov, X. Wang, I. Kamwa, and G. Joos, *An Approach to Constructing Analytical Energy Function for Synchronous Generator Models with Subtransient Dynamics*, IEEE Trans. Power Syst. **33**, 5958 (2018).
22. A. E. Motter, S. A. Myers, M. Anghel, and T. Nishikawa, *Spontaneous Synchrony in Power-Grid Networks*, Nat. Phys. **9**, 191 (2013).
23. Y. Kuramoto and D. Battogtokh, *Coexistence of Coherence and Incoherence in Nonlocally Coupled Phase Oscillators*, Physics (College. Park. Md). **4**, 380 (2002).
24. E. A. Martens, S. Thutupalli, A. Fourrière, and O. Hallatschek, *Chimera States in Mechanical Oscillator Networks*, Proc. Natl. Acad. Sci. U. S. A. **110**, 10563 (2013).
25. M. J. Panaggio and D. M. Abrams, *Chimera States: Coexistence of Coherence and Incoherence in Networks of Coupled Oscillators*, Nonlinearity **28**, R67 (2015).
26. L. Ding, F. M. Gonzalez-Longatt, P. Wall, and V. Terzija, *Two-Step Spectral Clustering Controlled Islanding Algorithm*, IEEE Trans. Power Syst. **28**, 75 (2013).
27. O. Ajala, A. Dominguez-Garcia, P. Sauer, and D. Liberzon, *A Second-Order Synchronous Machine Model for Multi-Swing Stability Analysis*, 51st North Am. Power Symp. NAPS 2019 (2019).
28. A. T. Winfree, *Biological Rhythms and the Behavior of Populations of Coupled Oscillators*, J. Theor. Biol. **16**, 15 (1967).
29. G. Chen, *Searching for Best Network Topologies with Optimal Synchronizability: A Brief Review*, IEEE/CAA J. Autom. Sin. **9**, 573 (2022).
30. C. Z. Karatekin and C. Uçak, *Sensitivity Analysis Based on Transmission Line Susceptances for Congestion Management*, Electr. Power Syst. Res. **78**, 1485 (2008).
31. S. Mei, Y. Ni, G. Wang, and S. Wu, *A Study of Self-Organized Criticality of Power System under Cascading Failures Based on AC-OPF with Voltage Stability Margin*, IEEE Trans. Power Syst. **23**, 1719 (2008).
32. I. Dobson, B. Carreras, V. Lynch, and D. Newman, *An Initial Model for Complex Dynamics in Electric Power System Blackouts*, Proc. Hawaii Int. Conf. Syst. Sci. 51 (2001).
33. T. Nishikawa and A. E. Motter, *Symmetric States Requiring System Asymmetry*, Phys. Rev. Lett. **117**, (2016).
34. F. Dörfler and F. Bullo, *Synchronization in Complex Networks of Phase Oscillators: A Survey*, Automatica **50**, 1539 (2014).
35. Y. Zou, T. Pereira, M. Small, Z. Liu, and J. Kurths, *Basin of Attraction Determines Hysteresis in Explosive Synchronization*, Phys. Rev. Lett. **112**, 114102 (2014).
36. D. R. Chialvo, *Emergent Complex Neural Dynamics*, Nat. Phys. **6**, 744 (2010).
37. H. Fan, Y. Wang, and X. Wang, *Eigenvector-Based Analysis of Cluster Synchronization in General Complex Networks of Coupled Chaotic Oscillators*, Front. Phys. **18**, (2023).
38. X. Li, W. Wei, and Z. Zheng, *Promoting Synchrony of Power Grids by Restructuring Network Topologies*, Chaos An Interdiscip. J. Nonlinear Sci. **33**, 63149 (2023).
39. Y. Zhang and A. E. Motter, *Symmetry-Independent Stability Analysis of Synchronization Patterns*, SIAM Rev. **62**, 817 (2020).
40. K. M. Amirthalingam and R. P. Ramachandran, *Improvement of Transient Stability of Power System Using Solid State Circuit Breaker*, Am. J. Appl. Sci. **10**, 563 (2013).
41. X. Liu, M. Shahidehpour, Y. Cao, Z. Li, and W. Tian, *Risk Assessment in Extreme Events Considering the Reliability of Protection Systems*, IEEE Trans. Smart Grid **6**, 1073 (2015).
42. R. Huang, Y. Chen, T. Yin, Q. Huang, J. Tan, W. Yu, X. Li, A. Li, and Y. Du, *Learning and Fast Adaptation for Grid Emergency Control* via *Deep Meta Reinforcement Learning*, IEEE Trans. Power Syst. **37**, 4168 (2022).
43. M. Guo, D. Xu, and L. Liu, *Design of Cooperative Output Regulators for Heterogeneous Uncertain Nonlinear Multiagent Systems*, IEEE Trans. Cybern. **52**, 5174 (2022).

 doi:10.20944/preprints202310.1791.v4

44. L. G. W. Roberts, A. R. Champneys, K. R. W. Bell, and M. Di Bernardo, *Analytical Approximations of Critical Clearing Time for Parametric Analysis of Power System Transient Stability*, IEEE J. Emerg. Sel. Top. Circuits Syst. **5**, 465 (2015).
45. R. Owusu-Mireku, H. D. Chiang, and M. Hin, *A Dynamic Theory-Based Method for Computing Unstable Equilibrium Points of Power Systems*, IEEE Trans. Power Syst. **35**, 1946 (2020).
46. A. Sajadi, R. W. Kenyon, and B. M. Hodge, *Synchronization in Electric Power Networks with Inherent Heterogeneity up to 100% Inverter-Based Renewable Generation*, Nat. Commun. **13**, 1 (2022).
47. M. Sun, Y. Feng, P. Wall, S. Azizi, J. Yu, and V. Terzija, *On-Line Power System Inertia Calculation Using Wide Area Measurements*, Int. J. Electr. Power Energy Syst. **109**, 325 (2019).
48. Y. Zhang, J. Bank, E. Muljadi, Y. H. Wan, and D. Corbus, *Angle Instability Detection in Power Systems with High-Wind Penetration Using Synchrophasor Measurements*, IEEE J. Emerg. Sel. Top. Power Electron. **1**, 306 (2013).
49. P. M. Anderson and A. A. Fouad, *Power System Control and Stability* (John Wiley & Sons, 2008).
50. A. Pai, *Energy Function Analysis for Power System Stability* (Springer Science & Business Media, 1989).